Eur Radiol (2007) 17: 541–551
DOI 10.1007/s00330-006-0384-1

Robert Werder
Daniel Nanz
Amelie M. Lutz
Dominik Weishaupt
Lucas McCormack
Burkhardt Seifert
Borut Marincek
Jürgen K. Willmann

Assessment of the abdominal aorta and its visceral branches by contrast-enhanced dynamic volumetric hepatic parallel magnetic resonance imaging: feasibility, reliability and accuracy

Received: 15 April 2006
Revised: 11 June 2006
Accepted: 23 June 2006
Published online: 1 September 2006

Robert Werder is a medical student at the School of Medicine, Zurich.

R. Werder · A. M. Lutz · D. Weishaupt · B. Marincek · J. K. Willmann
Institute of Diagnostic Radiology,
University Hospital Zurich,
Zurich, Switzerland

D. Nanz
Department of Medical Radiology,
University Hospital Zurich,
Zurich, Switzerland

Present address:
A. M. Lutz · J. K. Willmann (✉)
MIPS, Department of Radiology,
Stanford University,
E 150 Clark Center,
318 Campus Drive,
Palo Alto, CA 94305–5427, USA
e-mail: willmann@stanford.edu
Tel.: +1-650-7243642
Fax: +1-650-7244948

L. McCormack
Department of Visceral and Transplantation Surgery,
University Hospital Zurich,
Zurich, Switzerland

B. Seifert
Department of Biostatistics,
University of Zurich,
Zurich, Switzerland

Abstract The purpose of this study was to evaluate a new three-dimensional gradient-echo (GRE) MR sequence performed with a parallel acquisition technique to shorten breath-hold times (parallel GRE MRI) in the detection of arterial variants and stenosis of the abdominal aorta and its visceral branches. A total of 102 patients underwent dynamic parallel GRE MRI, timed to the arterial phase by a test bolus (mean breath-hold time, 17 s). For both quantitative and qualitative analysis, the abdominal aorta and its visceral branches were divided into 13 arterial segments. In a subanalysis of 55/102 patients, the accuracy of parallel GRE MRI compared to MDCT in the detection arterial variants and stenosis was calculated for two independent readers. Mean SNRs and CNRs were 47.2 and 35.6, respectively. Image quality was rated good or excellent in 1,234/1,326 segments (93%). Hepatic and renal arterial variants were identified with an accuracy of 93 and 95%, respectively (reader 1) and 98 and 100%, respectively (reader 2). Both readers detected arterial stenosis with an accuracy of 98%. Interobserver agreement was good to excellent for the detection of hepatic (κ=0.69) and renal (κ=0.92) variants and for the diagnosis of stenosis (κ=0.96). Dynamic three-dimensional parallel GRE MRI is feasible and allows a reliable and accurate diagnosis of arterial variants and stenosis of the abdominal aorta and its visceral branches in a short breath-hold-time.

Keywords Magnetic resonance imaging · Parallel imaging · Three-dimensional spoiled gradient-echo sequence · Liver · Abdominal aorta

Introduction

Dynamic magnetic resonance (MR) imaging has gained a major role in the diagnostic assessment of the liver, including the detection and characterization of focal liver lesions, the evaluation of diffuse liver diseases and the preoperative work-up before liver transplantation or resection. In addition to an evaluation of the liver parenchyma, a detailed preoperative knowledge of the anatomy of the abdominal aorta and its visceral branches is of paramount importance, since arterial complications still account for considerable morbidity and mortality in liver surgery [1, 2]. In many centers, multi-detector-row computed tomography (MDCT) angiography, a dedicated MR angiography or a

selective catheter digital subtraction angiography is performed as the next diagnostic step for an accurate preoperative assessment of the arterial abdominal anatomy in liver surgery candidates [3–6]. However, in an attempt to simplify and shorten the preoperative work-up, a comprehensive MR imaging protocol is desirable that combines the simultaneous evaluation of the hepatic parenchymal morphology with a detailed analysis of the abdominal vasculature.

With the introduction of dynamic three-dimensional (3D) gradient-echo (GRE) MR sequences with nearly isotropic pixel dimensions [7], robust 3D breath-hold MR visualization of the hepatic arteries in patients with liver disease has been shown feasible [8, 9]. However, breath-hold times exceeding 25–30 s are necessary for a standard 3D GRE MR sequence, thereby limiting the technique's utility in patients with compromised respiratory function [10].

Parallel MR imaging techniques use spatial information contained in the sensitivity profiles of the elements of a coil array [11–14]. This allows a reduction of the number of spatial encoding steps and, thus, a shortening of the MR acquisition time while preserving the spatial resolution of the MR image. In a preliminary study with 20 patients, the clinical feasibility of parallel MR imaging of the liver has been demonstrated by using a standard four-element body-array coil [10].

Liver acquisition with volume acceleration (LAVA) is a new 3D spoiled GRE sequence that incorporates the parallel MR imaging technique, thereby shortening the imaging time by a factor of two compared to conventional 3D GRE MR sequences of the liver (henceforth, this technique is referred to as parallel GRE MRI). In addition to a dynamic evaluation of the liver parenchyma, this sequence, in combination with a dedicated eight-element coil, can deliver high-quality angiographic views of an extended imaging volume that holds the whole abdominal aorta as well as its visceral branches and can be imaged in a short breath-hold time of less than 20 s.

The purpose of our study, therefore, was to evaluate retrospectively the feasibility, reliability and accuracy of parallel GRE MRI during dynamic liver parenchyma imaging in an assessment of the whole abdominal aorta and its visceral branches regarding the diagnosis of hepatic and renal arterial variants and stenosis in patients with liver disease.

Materials and methods

Patients

This study was performed in a retrospective manner and was approved by our hospital's institutional review board. Written informed consent was obtained from all patients.

During a 12-month period, 102 patients (57 men, mean age, 57 years; age range, 31–84 years; 45 women, mean age, 50 years; age range, 23–78 years) were referred to our institution for MR imaging of the liver. Clinical indications for MR imaging were the characterization of focal liver lesions in 85/102 patients (83%), preoperative assessment of the liver before liver transplantation in 11/102 patients (11%) and evaluation of hepatobiliary abnormality in 6/102 patients (6%). Liver cirrhosis was present in 38/102 patients (37%).

Of the 102 patients, 55 patients (29 men, mean age, 57 years; age range, 26–84 years; 26 women, mean age, 51 years; age range, 25–76 years) also underwent MDCT angiography of the aorta and its visceral arteries within 3 weeks of MR imaging. MDCT angiography was used as the standard of reference in our study for detection of hepatic and renal arterial variants as well as for diagnosis of arterial stenosis of the aorta and its visceral branches.

MR imaging

MR imaging was performed in all 102 patients using a 1.5-T MR system (Signa EchoSpeed Plus, GE Healthcare, Milwaukee, WI) with a maximum gradient amplitude of 33 mT/m and a slew rate of 120 mT/(m*ms). Patients were positioned supine and feet first on the scan table. For signal reception an anteroposterior eight-element phased-array surface coil was used covering the entire liver and the whole abdominal aorta.

For dynamic MRI, a parallel 3D spoiled GRE sequence (LAVA, Liver Acquisition with Volume Acceleration; GE Healthcare's 12.0M4 version) was obtained in the transverse plane using the following imaging parameters: TR/TE, 3.1/1.4 ms; excitation angle, 15°; receiver bandwidth, ±83.3 kHz; nominal measured voxel dimensions in acquisition along the frequency-, phase- and slice-encoding directions, respectively, $1.5\times1.5\times4.0$ mm^3; interpolated reconstructed voxel dimensions, $0.75\times0.75\times2.0$ mm^3; fat-suppression inversion-recovery time, 7.0 ms; 36 to 56 slices; number of excitations, 0.73. The parallel 3D spoiled GRE sequence achieved an acceleration by a factor of two by reducing the number of phase-encoding steps acquired along the anterior-posterior direction. The coil sensitivity profiles required for the sensitivity-encoding (SENSE) image reconstruction [12] were derived from a separate single breath-hold calibration scan that preceded the dynamic parallel MR scans. Spectrally selective fat-magnetization inversion pulses were repeatedly applied during the imaging sequence, which induced repeated zero-crossings of the fat signal. The flip angle was optimized to have one such zero-crossing temporally coincide with the acquisition of the center of the κ-space, which optimized the fat-signal suppression.

The sequence was applied in the arterial, portal venous and equilibrium phase following intravenous administration of 1.0 M gadobutrol (gadolinium-D03A-butriol,

Gadovist, Schering AG, Berlin, Germany) through a 20–22-gauge needle that was placed in an antecubital vein. Gadubutrol was administered at a dose of 0.1 mmol/kg bodyweight and at a flow rate of 2 ml/s by using a power injector (Spectris, Medrad, Indianola, PA). The contrast bolus was followed by a 20-ml saline flush administered at the same flow rate. Parallel GRE MRI was timed to capture the arterial phase, the portal venous phase and the equilibrium phase. The optimal delay time after the start of contrast medium injection for the arterial phase was determined individually for each patient by measuring the time needed by a test bolus of 1 ml gadobutrol to travel from the injection site to the abdominal aorta at the level of the celiac trunk with a multiphase sagittal single-section GRE sequence (repetition time, 5 ms; echo time, 1 ms; flip angle, 60°). Only the MR images acquired during the arterial phase of the contrast medium distribution were evaluated in this study.

The mean acquisition time of the parallel-GRE-MR data sets obtained during the contrast medium arterial phase was 17 s (range, 15–19 s). All parallel GRE MRIs were performed during breath holding at the end of inspiration.

MDCT imaging

In the subset of 55 patients who also underwent MDCT imaging of the abdomen for clinical reasons, MDCT scans were performed with a 16-detector row CT scanner (Sensation 16; Siemens, Forchheim, Germany).

The delay time between the start of contrast material administration and the start of scanning during the arterial phase of contrast medium was obtained for each patient individually by using a bolus-tracking technique (CARE-Bolus, Sensation 16 Navigator, Siemens, Forchheim, Germany); 120 ml of a nonionic iodinated contrast medium (iodixanol; Visipaque; Amersham Health, Buckinghamshire, England; 270 mg iodine per milliliter) was administered via a 20–22–gauge needle placed in an antecubital vein. The contrast medium was administered with an automated injector (Ulrich Medical AG, Ulm-Jungingen, Germany) at a flow rate of 4 ml/s followed by a 30 ml flush of saline administered at the same flow rate.

Data acquisition was performed in the arterial and portal venous phase with a nominal section thickness of 1.5 mm, a table-feed of 20 mm per rotation and a 0.5-s gantry rotation time (pitch, 0.8). The X-ray tube voltage setting was 120 κV at a mean tube current of 160 mA. Transverse sections were reconstructed with a slice thickness of 2 mm at an interval of 1 mm. The reconstruction field of view was 30 cm at a matrix size of 512×512. Only the MDCT scans obtained during the arterial phase of the contrast medium were evaluated in the study.

Image analysis

Images were quantitatively and qualitatively analyzed on a dedicated interactive workstation (Advantage Windows Workstation 4.2, GE Healthcare, Buc, France).

Quantitative analysis of MR imaging

In all 102 patients, measurements of signal-to-noise ratios (SNRs) and contrast-to-noise ratios (CNRs) were performed in random order by one of the authors who was blinded to all patient data. For this purpose, the abdominal aorta and its visceral branches were divided into 13 arterial segments including the celiac trunk, the common hepatic artery, the left gastric artery, the splenic artery, the gastroduodenal artery, the proper hepatic artery, the left and right hepatic arteries, the superior mesenteric artery, the right and left renal arteries, the inferior mesenteric artery and the infrarenal abdominal aorta. By using reader-defined regions of interest (ROI) in the arteries, adjacent structures (retroperitoneal fat or liver parenchyma) and background noise outside the body within the coil (air), SNR and CNR measurements were performed in a total of 1,319/1,326 arteries (99%; all arteries under consideration with moderate or better visibility; see below). ROIs were set to encompass as much as possible of the different arteries under consideration (mean, 20 mm^2; range, 5–160 mm^2). SNRs and CNRs were calculated as follows: SNR = mean signal intensity in the artery/standard deviation of the magnitude background signal outside the body within the coil (air); CNR = (mean signal intensity in the artery - mean signal intensity in the adjacent retroperitoneal fat or adjacent liver parenchyma)/standard deviation of the magnitude background signal outside the body within the coil (air) [8, 15, 16]. However, since noise is not spatially uniform in images obtained by parallel imaging reconstruction, comparisons with both SNR and CNR values from other studies are difficult and of limited value in many cases.

Qualitative analysis of MR imaging

Subjective image quality

In all 102 patients (a total of 1,326 arteries), the subjective image quality of the 13 arterial segments under consideration was assessed in random order on the parallel-GRE-MR images in a consensus reading by two blinded radiologists (readers 1 and 2). The image quality of each vessel was graded by using a four-point Likert scale: (1) poor visibility (diagnostic information cannot be obtained from the image because of severe blurring artifacts); (2) moderate visibility (image quality of vessel is degraded due to low signal intensity or moderate blurring artifacts); (3) good visibility

(high signal intensity, only slight blurring artifacts); (4) excellent visibility (high signal intensity, no blurring artifacts). Apart from the unavoidable increase of noise artifacts from the parallel imaging reconstruction, artifacts could be successfully eliminated in our study by selecting a field-of-view large enough to cover the complete anatomy in the anterior-posterior direction.

Variant visceral arterial anatomy

In all 102 patients, readers 1 and 2 independently performed a separate analysis of the parallel-GRE-MR images with regard to the presence of surgically important hepatic and renal arterial variants. Both readers were blinded to the results from MDCT imaging, and patients were presented in random order. Both readers were allowed to use the transverse source images and, if considered useful, transverse or oblique thick-slab maximum intensity projections of the parallel-GRE-MR data sets. Both readers were asked to classify hepatic artery anatomy into 1 of 10 types according to the Michels classification [17], plus an 11th type to include other variants not described in the Michels classification. In addition, both readers noted the presence and number of accessory left or right renal arteries as well as the presence of an early branching of the renal arteries (branching within 2 cm of the origin of the renal artery from the abdominal aorta) [18].

Arterial stenosis

Both readers were asked to notify independently the presence of arterial stenosis in all arteries under consideration. Grading of arterial stenosis was performed by using a four-point Likert scale: (1) normal vessel or mild vessel irregularities (<10% luminal narrowing); (2) moderate arterial stenosis (10–49% luminal narrowing); (3) severe arterial stenosis (50–99% luminal narrowing); (4) occlusion. Grading of the arterial stenosis was performed with an electronic caliper. Arterial stenosis with a grade of 3 or 4 was considered hemodynamically significant.

Analysis of MDCT angiography

Image analysis of MDCT angiography was performed in random order by a consensus panel consisting of one radiologist (reader 3) and one surgeon with experience in liver surgery (reader 4) on the basis of the transverse MDCT source data. If considered useful, both readers were also allowed to use transverse or oblique thick-slab maximum intensity projections of the MDCT data sets. The readers were blinded to all patient data, including the results from MR imaging. For assessment of hepatic and renal arterial variants as well as for grading of arterial stenosis of the abdominal aorta and its visceral branches, the same classification was used as for the evaluation of the parallel-GRE-MR images.

Statistical analysis

SNRs and CNRs are presented as means ± standard deviations. For an assessment of the reliability of parallel GRE MRI, interobserver agreements between readers 1 and 2 for the depiction of hepatic and renal arterial variants and for the detection of arterial stenosis were determined by calculating the κ values (poor, κ=0; slight, κ of 0.01–0.2; fair, κ of 0.21–0.40; moderate, κ of 0.41–0.60; good, κ of 0.61–0.80; excellent, κ of 0.81–1.00) [19].

In the subset of 55 patients with MDCT angiography sensitivities, specificities, positive and negative predictive values as well as accuracy including 95% confidence intervals (CI) of the parallel GRE MRI compared to MDCT angiography were calculated for readers 1 and 2 with regard to the detection of hepatic and renal arterial variants and regarding the detection of hemodynamically significant arterial stenosis of the aorta and its visceral branches. Since in all patients there was a maximum of one hemodynamically significant arterial stenosis, a per patient analysis was performed.

Results

Quantitative image analysis

Table 1 summarizes the means ± standard deviations of the SNRs and CNRs measured in the aorta and its visceral branches on parallel GRE MRI in all 102 patients.

Qualitative image analysis

Subjective image quality

Image quality was rated as excellent in 829/1,326 arteries (62%; Fig. 1), good in 405/1,326 arteries (31%) and fair in 85/1,326 arteries (6%) (Table 2). Seven of 1,326 arteries (1%) could not be depicted on parallel dynamic MRI (grade 1, poor visibility). Of the seven arteries with poor image quality on the MR images, there were five gastroduodenal arteries, as well as one right and one left hepatic artery.

Variant visceral arterial anatomy

The most common hepatic arterial variants were replaced right hepatic arteries arising from the superior mesenteric artery (Michels's type III) in 9/102 patients (9%; both readers) and replaced left hepatic artery arising from the

Table 1 Measurements of signal-to-noise and contrast-to-noise ratios for the abdominal aorta and its visceral branches on parallel gradient-echo magnetic resonance images in 102 patients

	Signal-to-noise ratio	Contrast-to-noise ratio
Celiac trunk	54.4±24.2	42.7±20.7
Splenic artery	51.0±22.8	38.9±18.1
Left gastric artery	37.9±21.5	26.7±16.5
Common hepatic artery	46.5±20.5	34.6±16.9
Gastroduodenal artery	33.7±18.2	21.9±14.4
Proper hepatic artery	42.4±17.9	28.8±13.1
Right hepatic artery	36.9±17.2	24.7±12.7
Left hepatic artery	35.5±16.0	27.6±32.3
Superior mesenteric artery	56.2±24.5	44.8±19.4
Right renal artery	50.0±22.2	38.6±17.8
Left renal artery	51.2±22.4	40.4±18.2
Infrarenal abdominal aorta	63.9±23.1	50.7±19.3
Inferior mesenteric artery	53.1±21.9	41.9±17.8
Total	47.2±21.0	35.6±18.2

Note: numbers are means ± standard deviations

left gastric artery (Michels's type II) in 3/102 patients (3%; reader 1) and 4/102 patients (4%; reader 2), respectively. Reader 1 did not detect an accessory left hepatic artery arising from the left gastric artery (type V), whereas reader

Table 2 Assessment of image quality of the abdominal aorta and its visceral branches on parallel gradient-echo magnetic resonance images of 102 patients

	Image quality of artery			
	Grade			
	1	2	3	4
Celiac trunk	0	0	30	72
Splenic artery	0	2	39	61
Left gastric artery	0	10	40	52
Common hepatic artery	0	4	41	57
Gastroduodenal artery	5	22	37	38
Proper hepatic artery	0	10	44	48
Right hepatic artery	1	17	39	45
Left hepatic artery	1	18	38	45
Superior mesenteric artery	0	0	19	83
Right renal artery	0	0	18	84
Left renal artery	0	1	18	83
Infrarenal abdominal aorta	0	0	20	82
Inferior mesenteric artery	0	1	22	79
Total	7	85	405	829

Note: grade 1, poor visibility (diagnostic information cannot be obtained from image because of severe blurring artifacts); grade 2, moderate visibility (image quality of vessel is degraded due to low signal intensity or moderate blurring artifacts); grade 3, good visibility (high signal intensity, only slight blurring artifacts); grade 4, excellent visibility (high signal intensity, no blurring artifacts)

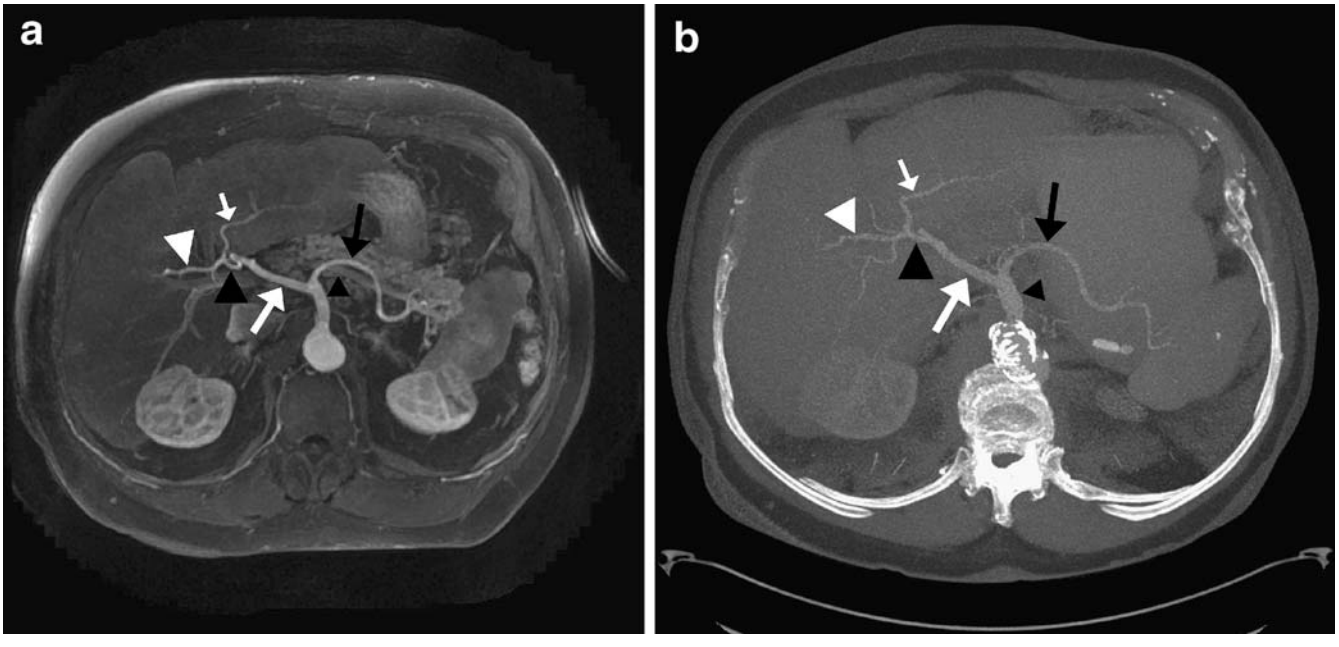

Fig. 1 Michels's type 1 hepatic arterial anatomy on parallel GRE MRI in a 79-year-old man, confirmed by contrast-enhanced multidetector row computed tomography (MDCT) imaging. On transverse thick-slab maximum intensity projection of parallel-GRE-MR (**a**) and MDCT (**b**) data sets, celiac trunk (*small black arrowhead*), splenic artery (*black arrow*), common hepatic artery (*large white arrow*), proper hepatic artery (*large black arrowhead*), as well as right (*large white arrowhead*) and left hepatic arteries (*small white arrow*) can be seen. Both readers graded image quality of all arteries as excellent on parallel GRE MRI

2 diagnosed a type-V hepatic arterial variant in 2/102 patients (2%) (Table 3).

According to both readers, 8/102 patients (8%; reader 1) and 4/102 patients (4%; reader 2), respectively, had hepatic arterial variants not included in the original description by Michels, which was classified as type XI in our study: direct origin of the left gastric artery from the aorta (*n*=5, reader 1; n=2, reader 2; Fig. 2), common hepatic artery arising directly from the aorta (*n*=1, both readers; Fig. 3), common hepatic artery arising directly from the aorta combined with replaced left hepatic artery from the left gastric artery (*n*=1; both readers), as well as right hepatic artery arising from the common hepatic artery proximal to the origin of the gastroduodenal artery (*n*=1; reader 1; *n*=0, reader 2). For all hepatic arterial variants, there was good interobserver agreement between both readers (κ=0.69; 95% CI: 0.56, 0.8).

Reader 1 detected accessory renal arteries in 20/102 patients (20%) and reader 2 in 21/102 patients (21%) (Fig. 4). Both readers diagnosed an early branching of the renal arteries in 15/102 patients [15%: in 14/15 patients (93%) on the left side and in 1/15 patients (7%) on the right side]. Overall, there was excellent interobserver agreement between both readers in the detection of renal arterial variants (κ=0.92; 95% CI: 0.79, 1.0).

The distribution of hepatic and renal arterial variants as identified on parallel-GRE-MR images compared to MDCT images in the subanalysis of 55 patients is presented in Table 4. MDCT imaging confirmed the presence of Michels's type V variants in two patients as diagnosed by reader 2, but not reported by reader 1. Overall, there was excellent agreement between parallel GRE MRI and MDCT for both readers with regard to the classification of hepatic and renal arterial variants. Based on the parallel GRE MRI, reader 1 agreed in 92.7% of the cases with the MDCT imaging regarding the classification of hepatic arterial variants (κ=0.82; 95% CI: 0.66, 0.98) and in 96.5% regarding the classification of renal arterial variants (κ=0.89; 95% CI: 0.7, 1.0). Reader 2 agreed with MDCT imaging in 94.6% based on parallel GRE MRI with regard to the classification of hepatic arterial variants (κ=0.87; 95% CI: 0.71, 1.0) and in 100% with regard to the classification of renal arterial variants (κ=1.0; 95% CI: 0.82, 1.0). Compared to MDCT, both readers detected the presence of hepatic and renal arterial variants with an accuracy between 93 and 100% (Table 5).

Table 3 Variant hepatic and renal artery anatomy as assessed by two independent readers on parallel-gradient-echo magnetic resonance images of 102 patients

Variant arterial anatomy	Parallel GRE MRI	
	Reader 1	Reader 2
Hepatic:		
I	78	79
II	3	4
III	9	9
IV	1	1
V	0	2
VI	0	0
VII	0	0
VIII	1	1
IX	2	2
X	0	0
XI	8	4
Renal:		
Bilateral single renal artery	82	81
Accessory right renal artery	9	8
Accessory left renal artery	7	9
Accessory right and left renal artery	3	2
Two accessory right renal arteries	0	1
Two accessory left renal arteries	1	1
Early branching right renal artery	1	1
Early branching left renal artery	14	14

Note: I-X are from the Michels classification [17]. XI is a designation for any arterial variant not described for types I-X. Early branching: branching within 2 cm of the origin of the renal artery from the abdominal aorta. GRE: gradient-echo; MRI: magnetic resonance imaging

Arterial stenosis

Reader 1 identified a grade 2 stenosis in 9/102 patients (9%; celiac trunk, 8 patients; superior mesenteric artery, 1 patient) and a grade 3 stenosis in 5/102 patients (5%; celiac trunk, 3 patients; superior mesenteric artery, 2 patients) on parallel-GRE-MR images. In 8/102 patients (8%; celiac trunk, 6 patients; superior mesenteric artery, 2 patients), reader 2 detected a grade 2 stenosis, and in 5/102 patients (5%; celiac trunk, 3 patients; superior mesenteric artery, 2 patients), a grade 3 arterial stenosis was diagnosed. Overall, there was an excellent interobserver agreement between reader 1 and 2 in the detection of arterial stenosis (κ=0.96; 95% CI: 0.8, 1.0). Accuracy of parallel GRE MRI compared to MDCT was 98% (95% CI: 90%, 100%) for both readers with regard to the diagnosis of hemodynamically significant stenosis (Table 5; Fig. 5).

Discussion

With the recent introduction of parallel imaging techniques, the time for data acquisition in clinical MRI can be significantly reduced. Parallel imaging techniques exploit the coil sensitivities of multiple independent coil elements to permit under-sampling in the phase-encoding direction. This process substantially reduces the time for MR data acquisition, resulting in shorter overall examination times without compromising spatial resolution [11–14].

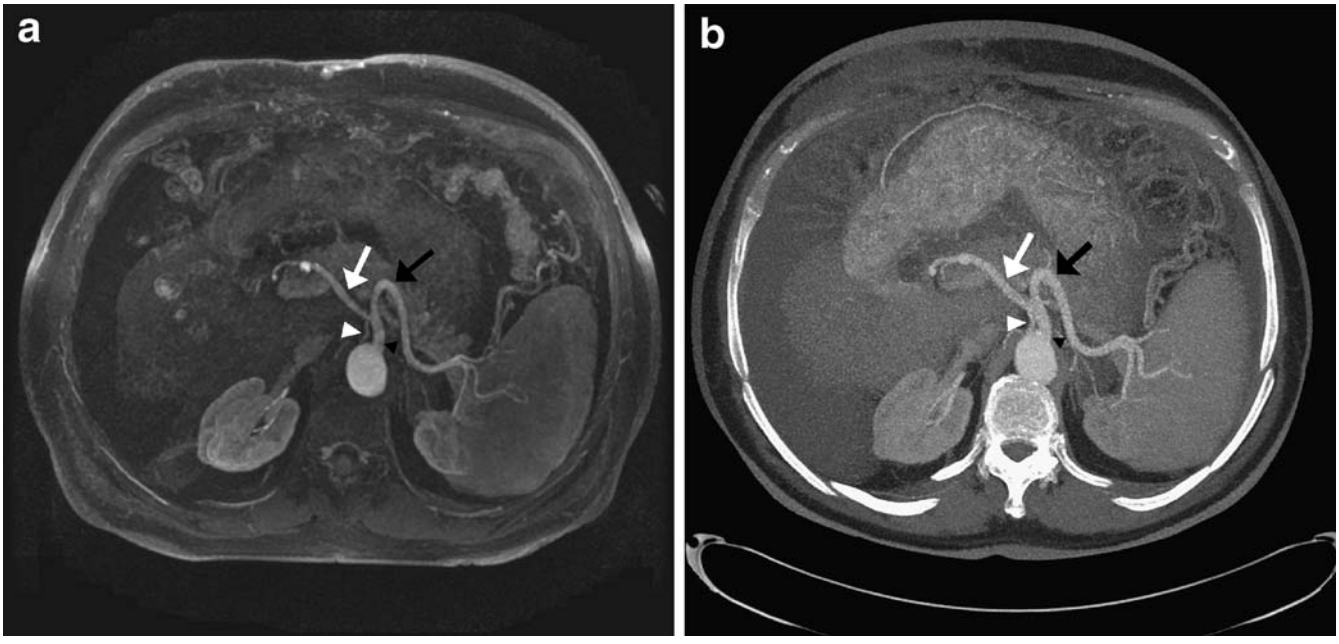

Fig. 2 A 62-year-old man with a variant anatomy of the celiac trunk. On transverse thick-slab maximum intensity projection of parallel-GRE-MR data set (**a**) both readers depicted a left gastric artery (*small white arrowhead*) arising directly from the abdominal aorta, which was confirmed on transverse thick-slab maximum intensity projection of MDCT data set obtained in the same patient (**b**). Note celiac trunk (*small black arrowhead*), splenic artery (*black arrow*), as well as common hepatic artery (*white arrow*)

For dynamic contrast-enhanced MRI of the liver, fast imaging techniques are desirable: In addition to liver parenchymal imaging, dynamic contrast-enhanced MRI is considered to provide detailed information about the anatomy of the abdominal aorta and its visceral branches for accurate surgical planning of liver resection or hepatic transplantation, or for planning of catheter-related interventional procedures such as chemoembolization [8, 9]. However, breath-hold times longer than 25 to 30 s are necessary for conventional 3D GRE MRI of the entire liver and abdominal aorta, and patients with liver disease are often not capable of holding their breath this long [10].

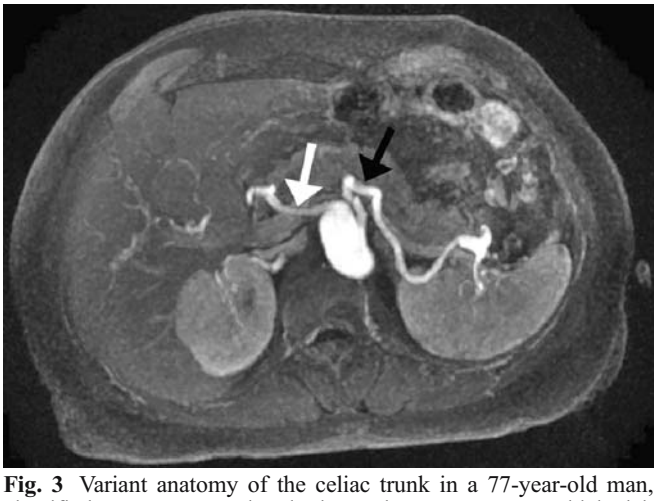

Fig. 3 Variant anatomy of the celiac trunk in a 77-year-old man, classified as type XI by both readers. Transverse thick-slab maximum intensity projection of parallel-GRE-MR data set at the level of the celiac trunk demonstrates separate origin of the common hepatic artery (*white arrow*) from the abdominal aorta. The left gastric artery (not shown) arises from the celiac trunk. Splenic artery (*black arrow*)

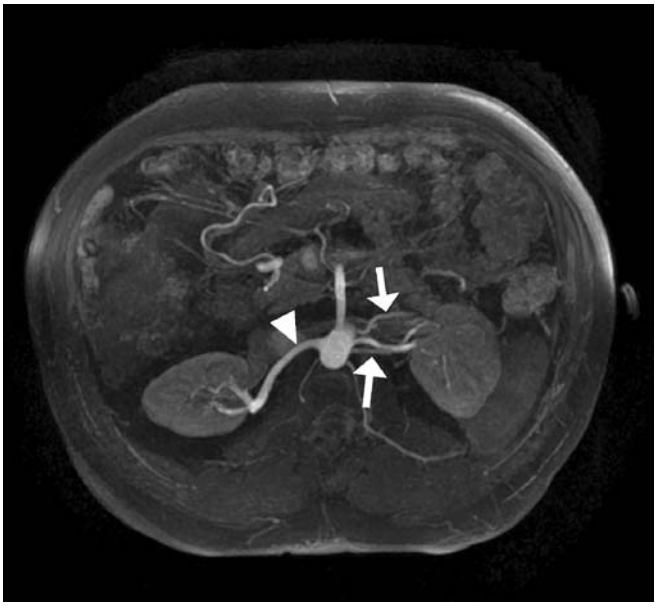

Fig. 4 A 59-year-old man with two accessory left renal arteries (*arrows*) and a single right renal artery (*arrowhead*), noted by both readers on transverse thick-slab maximum intensity projection of parallel-GRE-MR data set

Table 4 Variant hepatic and renal artery anatomy as assessed by two independent readers on parallel-gradient-echo magnetic resonance images in a subset of 55 patients compared to multi-detector row computed tomography angiography

Variant arterial anatomy	MDCT angiography	Parallel GRE MRI	
		Reader 1	Reader 2
Hepatic:			
I	40	44	43
II	3	2	2
III	6	5	4
IV	0	0	0
V	2	0	2
VI	0	0	0
VII	0	0	0
VIII	1	1	1
IX	1	1	1
X	0	0	0
XI	2	2	2
Renal:			
Bilateral single renal artery	44	46	44
Accessory right renal artery	5	5	5
Accessory left renal artery	4	3	4
Accessory right and left renal artery	1	1	1
Two accessory right renal arteries	1	0	1
Two accessory left renal arteries	0	0	0
Early branching right renal artery	0	0	0
Early branching left renal artery	6	6	6

Note: I-X are from the Michels classification [17]. XI is a designation for any arterial variant not described for types I-X. Early branching: branching within 2 cm of the origin of the renal artery from the abdominal aorta. MDCT: multi-detector row computed tomography; GRE: gradient-echo; MRI: magnetic resonance imaging

In a recent study, McKenzie et al. [10] demonstrated the clinical feasibility of a 3D GRE MR sequence with parallel imaging for shortening of MR data acquisition of the liver by a factor of two while preserving acceptable image quality. In 20 patients with hepatobiliary disease, the mean time for MRI of the liver with parallel imaging was 13 s compared to 26 s without parallel imaging [10]. The accelerated MR data acquisition with parallel imaging resulted in gains of image quality of abdominal anatomical structures in a subset of three patients with limited breath-hold capability in this study [10]. However, to the best of our knowledge, the feasibility, reliability and accuracy of dynamic 3D GRE MRI, performed with a parallel acquisition technique, have not been evaluated so far for

Table 5 Performance of parallel-gradient-echo magnetic resonance images as assessed by two independent readers compared to multi-detector row computed tomography angiography in the detection of presence of hepatic and renal arterial variants and in the detection of hemodynamically significant arterial stenosis in a subset of 55 patients

	True-positive findings		True-negative findings		False-positive findings		False-negative findings		Sensitivity (%)		Specificity (%)		PPV (%)		NPV (%)		Accuracy (%)	
	Reader 1	Reader 2	Reader 1	Reader 2	Reader 1	Reader 2	Reader 1	Reader 2	Reader 1	Reader 2	Reader 1	Reader 2	Reader 1	Reader 2	Reader 1	Reader 2	Reader 1	Reader 2
Hepatic variant	11	12	40	40	0	0	4	3	73 (45,93)	80 (52,96)	100 (91,100)	100 (91,100)	100 (72,100)	100 (74,100)	91 (78,97)	93 (81,99)	93 (82,98)	95 (85,99)
Renal variant	10	11	44	44	0	0	1	0	91 (59,100)	100 (72,100)	100 (92,100)	100 (92,100)	100 (70,100)	100 (72,100)	98 (88,100)	100 (92,100)	98 (90,100)	100 (94,100)
Arterial stenosis	3	3	51	51	1	1	0	0	100 (16,100)	100 (16,100)	98 (90,100)	98 (90,100)	75 (12,100)	75 (12,100)	100 (93,100)	100 (93,100)	98 (90,100)	98 (90,100)

Note: numbers in parentheses are 95% CI. PPV: positive predictive value; NPV: negative predictive value

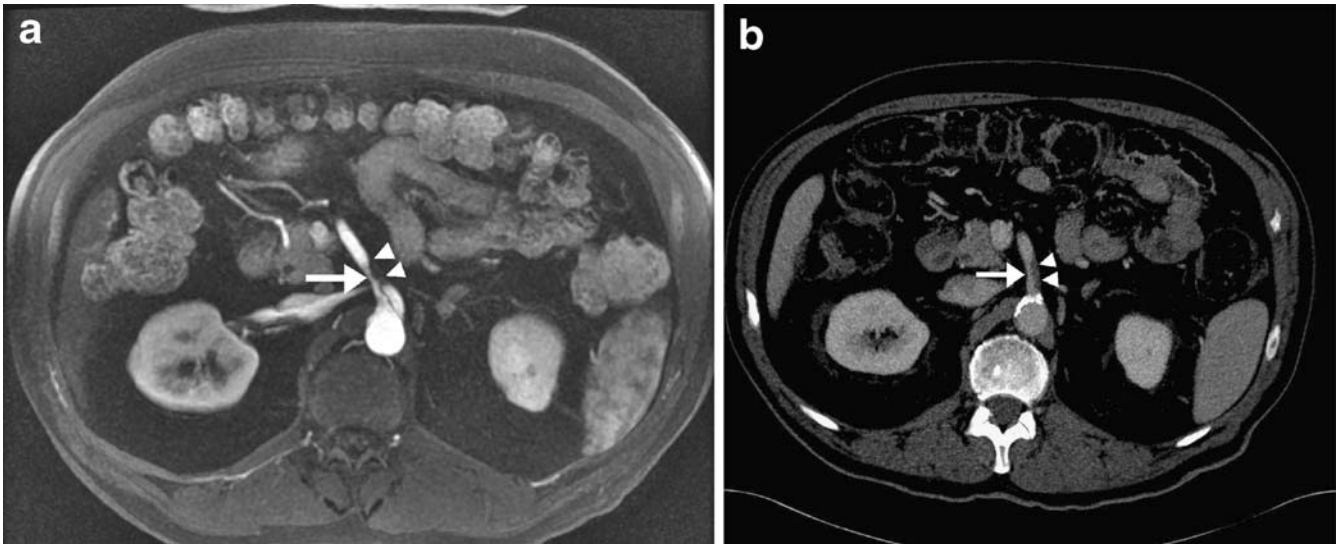

Fig. 5 (**a**) A 78-year-old man with stenosis of the superior mesenteric artery (*arrow*) that was graded as hemodynamically significant (grade 3) by both readers on transverse thick-slab maximum intensity projection of parallel-GRE-MR data set acquired in the arterial phase of the contrast medium. (**b**) Grade 3 stenosis of superior mesenteric artery (*arrow*) was confirmed on transverse thick-slab maximum intensity projection of MDCT data set obtained in the same patient. Note obstructing, non-calcified atheroscleotic plaque (*arrowheads*) in the superior mesenteric artery

detection of arterial variants and stenosis of the abdominal aorta and its visceral branches in a large number of patients.

Our study demonstrates good feasibility of dynamic parallel GRE MRI for visualization of the abdominal aorta and its visceral branches in 102 patients with liver disease. Timed to the arterial phase of the extracellular contrast medium distribution, the image quality of parallel GRE MRI was good or excellent for 93% of 1,326 arterial segments under consideration. In particular, the small arteries including the right and left hepatic arteries, the gastroduodenal artery, as well as the inferior mesenteric artery were depicted with good mean image quality. Only in 7 of the 1,326 arterial segments (1%) was the image quality rated non-diagnostic by both readers. Non-diagnostic image quality was caused by motion artifacts in all of these seven arteries.

Good or excellent visibility of the abdominal aorta and its visceral branches on parallel GRE MRI is also reflected by the high SNRs and CNRs measured for the different abdominal arteries under consideration in our study. It has been estimated that SNRs and CNRs of MR images acquired with parallel imaging are reduced by about 30% for an acceleration factor of two compared to conventional 3D GRE MRI without parallel imaging [20]. Interestingly, SNRs and CNRs for the aorta and its visceral branches measured in our study were comparable or even higher than reported values on conventional 3D GRE MRI using the same definitions for calculation [8, 15]. There may be at least three explanations for the comparatively high SNR and CNR values obtained in our study. The eight-element phased-array surface coil used in our study is designed for optimized SNRs in parallel imaging of the abdomen. It integrates preamplifiers into the coil and, thus, provides signal-preamplification as close as possible to the signal-receiving loops. Furthermore, the geometric arrangement of its coil elements is optimized to keep the noise-enhancing geometry factor g (which determines local noise variations in parallel imaging) as low as possible throughout the imaging volume, which could be kept large enough to include the liver and the whole abdominal aorta with its visceral branches in our study. Second, in all examinations of our study, 1-molar gadolinium-chelate gadubutrol was administered in contrast to 0.5-molar gadopentetate dimeglumine in the aforementioned studies [8, 15]. Gadubutrol has been shown to improve SNRs and CNRs in aortoiliac angiography by 40–70% compared to gadopentetate dimeglumine [21, 22]. This improvement of signal intensity may result from the higher r1/r2 molar relaxivity ratio of gadubutrol compared to that of gadopentetate dimeglumine, which may also lead to a reduction of interfering T2* effects during the arterial first pass of the contrast medium [22]. Third, the first pass of the extracellular contrast medium may have been captured better due to the faster data acquisition of the parallel MRI compared to conventional 3D MRI without parallel imaging.

However, when discussing the high SNRs and CNRs measured in our study, the following needs to be considered. The image reconstruction process in parallel MRI causes the noise to fluctuate in the image. Its magnitude strongly depends on the distance between a voxel of interest and the coil elements of the phased-array surface coil and it typically increases with increasing distances [23]. Thus, in case of abdominal MRI, noise is

typically larger in regions deep inside the body (i.e., the abdominal aorta and its visceral branches) than in regions closer to the body surface or the phased-array surface coil. When measuring the signal intensity and the noise at different locations (e.g., the signal intensity in the aorta and the noise in the air outside the body within the coil), this introduces a systematic error into the SNR and CNR measurements. Therefore, we hypothesize that both SNRs and CNRs may be overestimated in our study.

In patients who undergo liver transplantation or partial resection of the liver, patency of all hepatic arterial branches is mandatory for the survival of the graft or the remnant liver parenchyma. Therefore, careful analysis of the hepatic arterial anatomy prior to liver surgery is important. The results of the study show that parallel GRE MRI is accurate and reliable for the diagnosis of hepatic arterial variants. Compared to MDCT angiography as the standard of reference, both readers detected hepatic arterial variants with an accuracy of over 90% and with an excellent interobserver agreement.

Liver surgery may be complicated very rarely by an aberrant hepatic artery from the right renal artery [2]. Since there was no aberrant hepatic artery from the renal arteries in our study, other surgically important variants including the presence of accessory renal arteries or of an early branching of the renal arteries were used to assess the performance of contrast-enhanced parallel GRE MRI for the detection of renal arterial abnormalities [18, 24]. Our study demonstrates that the whole course of the renal arteries can be evaluated with good or excellent image quality on most MR images. Accessory renal arteries and the presence of an early branching of the renal arteries were depicted with high sensitivity and specificity, respectively, by both readers.

Apart from assessment of hepatic and renal arterial variants, accurate preoperative knowledge of arterial stenosis in patients with liver disease is important. For example, a severe stenosis of the celiac trunk precludes the placement of an intraarterial catheter into the gastroduodenal or hepatic artery for selective preoperative intraarterial chemotherapy. In addition, other procedures including partial liver donation or transarterial chemoembolization of the liver can be jeopardized in patients with arterial stenosis. Hemodynamically significant arterial stenoses in the celiac trunk and superior mesenteric artery were detected with an accuracy of 98% by both readers on parallel-GRE-MR images compared to the standard of reference. The high reliability of parallel GRE MRI in the detection of any grade of arterial stenosis is mirrored by the overall excellent interobserver agreement in our study.

The introduction of the parallel-GRE-MR sequence into the clinical routine may be a further step towards a shorter and simplified preoperative work-up of liver surgery candidates. In addition to liver parenchymal imaging, parallel GRE MRI timed to the arterial phase of contrast medium may be used for an accurate preoperative assessment of the aorta and its visceral branches without the need of an additional imaging procedure for a dedicated evaluation of the arterial anatomy. In particular in patients with compromised respiratory function, parallel GRE MRI is valuable due to the acquisition times of below 20 s per dynamic data acquisition.

The following limitations of our study need to be acknowledged. First, MDCT angiography was available as a standard of reference in only 55 of the 102 patients in our study. Additionally, due to the still comparatively large acquired slice thickness of 4 mm, quantification of area stenosis in small vessels that require reformations of the data set may be of insufficient accuracy with the current technique. Finally, there was a low prevalence of hemodynamically significant arterial stenosis in the patients with available MDCT angiography in our study. This may limit the calculated statistics for parallel GRE MRI with regard to the detection of hemodynamically significant arterial stenosis.

In conclusion, results of this study have shown that parallel-GRE-MRI allows a reliable assessment of the abdominal aorta and its visceral branches during dynamic liver parenchymal imaging. Compared to MDCT angiography as a standard of reference, the presence of hepatic and renal arterial variants and stenosis can be predicted with high accuracy.

References

1. Ishigami K, Zhang Y, Rayhill S, Katz D, Stolpen A (2004) Does variant hepatic artery anatomy in a liver transplant recipient increase the risk of hepatic artery complications after transplantation? AJR Am J Roentgenol 183:1577–1584
2. Braun MA, Collins MB, Wright P (1991) An aberrant right hepatic artery from the right renal artery: anatomical vignette. Cardiovasc Intervent Radiol 14:349–351
3. Takahashi S, Murakami T, Takamura M et al (2002) Multi-detector row helical CT angiography of hepatic vessels: depiction with dual-arterial phase acquisition during single breath hold. Radiology 222:81–88
4. Stemmler BJ, Paulson EK, Thornton FJ, Winters SR, Nelson RC, Clary BM (2004) Dual-phase 3D MDCT angiography for evaluation of the liver before hepatic resection. AJR Am J Roentgenol 183:1551–1557

5. Kopka L, Rodenwaldt J, Vosshenrich R et al (1999) Hepatic blood supply: comparison of optimized dual phase contrast-enhanced three-dimensional MR angiography and digital subtraction angiography. Radiology 211:51–58
6. Sahani D, Mehta A, Blake M, Prasad S, Harris G, Saini S (2004) Preoperative hepatic vascular evaluation with CT and MR angiography: implications for surgery. Radiographics 24:1367–1380
7. Rofsky NM, Lee VS, Laub G et al (1999) Abdominal MR imaging with a volumetric interpolated breath-hold examination. Radiology 212:876–884
8. Lee VS, Lavelle MT, Rofsky NM et al. (2000) Hepatic MR imaging with a dynamic contrast-enhanced isotropic volumetric interpolated breath-hold examination: feasibility, reproducibility, and technical quality. Radiology 215:365–372
9. Lavelle MT, Lee VS, Rofsky NM, Krinsky GA, Weinreb JC (2001) Dynamic contrast-enhanced three-dimensional MR imaging of liver parenchyma: source images and angiographic reconstructions to define hepatic arterial anatomy. Radiology 218:389–394
10. McKenzie CA, Lim D, Ransil BJ et al (2004) Shortening MR image acquisition time for volumetric interpolated breath-hold examination with a recently developed parallel imaging reconstruction technique: clinical feasibility. Radiology 230:589–594
11. Sodickson DK, Manning WJ (1997) Simultaneous acquisition of spatial harmonics (SMASH): fast imaging with radiofrequency coil arrays. Magn Reson Med 38:591–603
12. Pruessmann KP, Weiger M, Scheidegger MB, Boesiger P (1999) SENSE: sensitivity encoding for fast MRI. Magn Reson Med 42: 952–962
13. Griswold MA, Jakob PM, Heidemann RM et al (2002) Generalized autocalibrating partially parallel acquisitions (GRAPPA). Magn Reson Med 47:1202–1210
14. Heidemann RM, Ozsarlak O, Parizel PM et al (2003) A brief review of parallel magnetic resonance imaging. Eur Radiol 13:2323–2337
15. Chen Q, Quijano CV, Mai VM et al (2004) On improving temporal and spatial resolution of 3D contrast-enhanced body MR angiography with parallel imaging. Radiology 231: 893–899
16. Vogt FM, Antoch G, Hunold P et al (2005) Parallel acquisition techniques for accelerated volumetric interpolated breath-hold examination magnetic resonance imaging of the upper abdomen: assessment of image quality and lesion conspicuity. J Magn Reson Imaging 21:376–382
17. Michels NA (1955) Blood supply and anatomy of the upper abdominal organs with a descriptive atlas. Philadelphia PL, 64–69
18. Rusnack D, Israel GM (2004) Kidney transplantation: evaluation of donors and recipients. Magn Reson Imaging Clin N Am 12:505–514; vi–vii
19. Landis JR, Koch GG (1977) An application of hierarchical kappa-type statistics in the assessment of majority agreement among multiple observers. Biometrics 33:363–374
20. Glockner JF, Hu HH, Stanley DW, Angelos L, King K (2005) Parallel MR imaging: a user's guide. Radiographics 25:1279–1297
21. Goyen M, Lauenstein TC, Herborn CU, Debatin JF, Bosk S, Ruehm SG (2001) 0.5 M Gd chelate (Magnevist) versus 1.0 M Gd chelate (Gadovist): dose-independent effect on image quality of pelvic three-dimensional MR-angiography. J Magn Reson Imaging 14:602–607
22. Herborn CU, Lauenstein TC, Ruehm SG, Bosk S, Debatin JF, Goyen M (2003) Intraindividual comparison of gadopentetate dimeglumine, gadobenate dimeglumine, and gadobutrol for pelvic 3D magnetic resonance angiography. Invest Radiol 38:27–33
23. Wiesinger F, Boesiger P, Pruessmann KP (2004) Electrodynamics and ultimate SNR in parallel MR imaging. Magn Reson Med 52:376–390
24. Leiner T, de Haan MW, Nelemans PJ, van Engelshoven JM, Vasbinder GB (2005) Contemporary imaging techniques for the diagnosis of renal artery stenosis. Eur Radiol 15:2219–2229